RSC Advances

PAPER

View Article Online
View Journal | View Issue

Cite this: *RSC Adv.*, 2024, **14**, 3611

Exploring g-C_3N_4 as a green additive for biodegradable poly(butylene adipate-*co*-terephthalate) film with enhanced UV shielding and mechanical properties†

Maolin Zhang,[a] Yining Zhang,[a] Qi Liu,[a] Wen-Qing He*[ab] and Jialei Liu *[a]

Typical small organic dyes exhibit excellent UV absorption capabilities and are commonly used as additives to shield plastic films from photoaging. However, their tendency to decompose easily and migrate rapidly within a polymer matrix limits their service life. Herein we prepared g-C_3N_4 nanosheets and fabricated g-C_3N_4/PBAT films to investigate the effects of g-C_3N_4 on UV shielding and plasticizing of a biodegradable PBAT film. Photophysical characterizations revealed that an improved UV light barrier performance was achieved on g-C_3N_4/PBAT films compared to pure PBAT. Furthermore, the photoaging results show that g-C_3N_4 can stably exist in the PBAT matrix, enabling the aged g-C_3N_4/PBAT films to maintain their effective UV shielding ability, whereas the aged benzophenone (UV-0)/PBAT film shows a substantial decrease in UV light absorption due to the photodecomposition of UV-0. Additionally, g-C_3N_4 acted as a reinforcing material for PBAT, as evidenced by the approximately 1.5-fold increase in longitudinal tear strength and 1.6-fold increase in tensile strength of g-C_3N_4/PBAT films compared to pure PBAT. Remarkably, even after 100 hours of photoaging, the aged g-C_3N_4/PBAT films retained their favorable mechanical properties. This study highlights the potential of g-C_3N_4 as a new type of UV shield additive for future practical applications in protecting biodegradable plastic from photoaging.

Received 31st October 2023
Accepted 14th January 2024

DOI: 10.1039/d3ra07407b

rsc.li/rsc-advances

Introduction

Synthetic polyolefin plastics, such as polyethylene and polypropylene, have become indispensable in various facets of modern society. One can find polyolefin plastic in the fields of packaging, construction, automotives, agriculture, and many more.[1] In agriculture, polyolefin plastics are mainly used as a mulching and greenhouse film, which largely promotes agricultural efficiency by regulating the growth environment of crops, including sunlight, temperature, gas, and water.[2] Of them, in China, mulching film contributed 57.3% of agricultural plastic in 2019 according to the data from the China Rural Statistics Yearbook. Even now, the demand for the mulching film is still growing. Although we gain many benefits from mulching film, the current management strategies for spent mulching film are not sustainable, raising the concern of plastic pollution in the agricultural ecosystem.[3] The increasing awareness of the related environmental and health threats motivates researchers to seek solutions. One approach is to replace the persistent polyolefin plastics with aliphatic and aliphatic–aromatic polyester plastics, such as poly(lactic acid) (PLA), polycaprolactone (PCL), PHA poly(hydroxy alkanoates) (PHA), and poly(butylene adipate-terephthalate) (PBAT). These materials offer biodegradability and hydrolysis of ester bonds to non-toxic substances.[4,5] Among them, PBAT shows its advantages of affordability, ductility, and processability over the other three, leading to its widespread commercialization and market growth.[6] However, like other biodegradable plastics, PBAT has the drawback of poor photostability when exposed to sunlight, resulting in the deterioration of mechanical properties, which calls for further modification to realize anti-photoaging.[7]

To enhance the photostability and further elongate the functional lifespan of PBAT and other plastics, strategies like adding UV absorbers have been introduced and demonstrated as an effective way to protect the plastic from photo degrading.[8–10] Typically, commercially available organic chromophores like benzophenone,[11,12] benzotriazole,[8,13–15] triazine,[16] and their derivatives were well-developed as commercialized organic UV absorbers.[17] These absorbers offer UV blocking across the entire UV light spectrum. However, the low molecular weight of these UV absorbers usually brings a high mobility within the polymer matrix, resulting in a short protection time. Moreover, these UV absorbers are synthesized from petroleum and show negative

[a]*Institute of Environment and Sustainable Development in Agriculture, Chinese Academy of Agricultural Sciences, Beijing 100081, China. E-mail: hewenqing@cass.cn; liujialei@mail.ipc.ac.cn*

[b]*Institute of Western Agriculture, Chinese Academy of Agricultural Sciences, Changji, Xinjiang Uygur Autonomous Region, 831100, China*

† Electronic supplementary information (ESI) available. See DOI: https://doi.org/10.1039/d3ra07407b

effects on the environment when leaked out. In view of this, great efforts have been devoted to increasing their stability by modifying them with a steric group or grafting them onto a polymer backbone. However, the tedious synthetic procedures render them uneconomical. Besides, inorganic metal oxide semiconductors, such as TiO_2,[18] ZnO,[19] and CeO_2 (ref. 20) were also investigated as plastic UV absorbers. Whereas, their limited UV absorb ability, photocatalytic effect, and poor compatibility with the polymer matrix are still far from the demand for the application. To meet the demand for PBAT anti-photoaging, developing a new type of UV absorber is highly necessary.

In recent decades, graphene with high thermal stability, chemical stability, and good mechanical properties have garnered significant attention as a gas barrier or reinforcement for polymer composites.[21,22] In addition, graphene or graphene oxide was developed as the UV shield to protect polymer from photoaging due its UV light absorption and reflecting properties.[23,24] Similarly, graphitic carbon nitride (g-C_3N_4) is another type of two-dimensional materials, also got investigated in the field of reinforcement additive for polymer matrix.[25–28] In compared with graphene or graphene oxide, g-C_3N_4 has better good UV-Vis light absorption ability (a moderate band gap of 2.7–2.8 eV).[29] Furthermore, g-C_3N_4 can be prepared from inexpensive resources, such as melamine, urea, and cyanamide, through one-pot pyrolyzing method, endowing it with an "earth-abundant" nature. While the production of graphene or graphene oxide from graphite usually need tedious and/or environment-unfriendly methods. Given the above characteristics of g-C_3N_4, we hypothesized that, as green materials, g-C_3N_4 has the potential to serve as a new type of anti-photoaging additive for PBAT. To the best of our knowledge, no reports about g-C_3N_4 being used as a PBAT anti-photoaging additive. Herein, as a proof-of-concept experiment, g-C_3N_4 nanosheets were first prepared by pyrolyzing a mixture of melamine and NH_4Cl under the N_2 atmosphere at 550 °C, with a mass ratio of 1 : 4. Subsequently, two types of g-C_3N_4 nanosheet-doped PBAT films with different loading amounts of g-C_3N_4 were prepared using the casting film method. Pure PBAT and 2,4-dihydroxybenzophenone (UV-0)/PBAT film was also prepared for comparison. Experiment results show that the doped g-C_3N_4 nanosheets effectively shield UV light, similar to UV-0. However, the g-C_3N_4/PBAT films possess enhanced mechanical properties and long-term photostability compared to UV-0/PBAT films.

Experimental section

Regents and equipment

All chemicals were commercially available unless mentioned otherwise. Melamine (98%), NH_4Cl (98%), 2,4-dihydroxybenzophenone (99%), and talc powder were purchased from Tianjin Heowns Chemical Technology Co., Ltd. Poly(butylene adipate-terephthalate) (PBAT) was purchased from the Jinhui Zhaolong High-tech Co., Ltd, Shanxi, China. Casting film machine 1611-25/30CV was purchased from Labtech Engineering Co., Ltd. Pelletizer 1604-120/VS was purchased from Engineering Co., Ltd. Tubular furnace (BTF-1200C-S) was purchased from the Anhui BEQ Equipment Technology Co., Ltd. Tensile test machine (model STC-50 kg) was purchased from Jinan Labthink electromechanical Technology Co., Ltd. Xenon Aging Test Chamber (model BGD 860) was purchased from BIUGED Laboratory Instruments Co., Ltd.

Preparation of g-C_3N_4. g-C_3N_4 used in this work was prepared based on a previous study with a minor modification.[30] In detail, 5 g melamine, and 20 g NH_4Cl were uniformly mixed in an agate mortar and transferred the mixture to a crucible with a cover. Then the crucible was put to a tubular furnace and heated to 550 °C in a nitrogen atmosphere with a ramping rate of 2 °C min^{-1} for 4 h. After cooling to room temperature, a light yellow powder was obtained in a 50% yield.

Preparation of films PBAT, UV-0 (0.25)/PBAT, UV-0 (0.5)/PBAT, g-C_3N_4 (0.25)/PBAT, and g-C_3N_4 (0.5)/PBAT. Taking pure PBAT film as an example, 1 kg of the purchased PBAT precursors were first evenly mixed with 20 g talc powder by the vertical mixer. Then the mixture was loaded on the pelletizer for pelletizing, the temperature was set at 180 °C and the screw speed was 170 rpm. The PBAT master batch was obtained by granulating. By using the PBAT master batch, PBAT film was prepared in a casting film machine, the temperature was set at 160 °C, and the screw speed was 40 rpm. In a similar procedure, films UV-0 (0.25)/PBAT, UV-0 (0.5)/PBAT, g-C_3N_4 (0.25)/PBAT, and g-C_3N_4 (0.5)/PBAT were also prepared, the difference is that 2.5 g or 5 g of UV-0 or g-C_3N_4 was added to the mixture before pelleting.

Characterization

The morphologies of the prepared g-C_3N_4 were analyzed by an FEI Talos F200X transmission electron microscopy (TEM) at an operating voltage of 200 kV. The surface morphologies of the prepared films in this work were investigated by a ZEISS Gemini 300 scanning electron microscopy (SEM) with an acceleration voltage of 30 kV. Before collecting, the films were frozen in liquid nitrogen and coated with gold. X-ray diffraction (XRD) patterns were recorded by Bruker D8 focus powder diffractometer with a monochromator Cu Kα source operated at 40 kV and 30 mA. Thermogravimetric analysis (TGA) of the prepared films was carried out by an STA 449 F3/F5 thermal analyzer from 25 to 600 °C at a heating rate of 10 °C min^{-1} in the N_2 atmosphere. The ultraviolet-visible diffuse reflectance spectrum (UV-Vis DRS) was measured on a UH4150 Spectrophotometer (Integrating Sphere) in the 200–800 nm range. Fourier transforms infrared (FT-IR) spectroscopy was collected on a Nicolet IS10 FTIR spectrometer in the 400–4000 cm^{-1} range by using the KBr disk method. The thickness and mechanical properties of the prepared films were analyzed by an Auto Tensile Tester (Labthink, China, model: STC-50 kg). UV light-resistant properties of the prepared films were studied on a Xenon Aging Test Chamber (BIUGED, China, model: BGD 860) with a UV-340 lamp and a water spray system. The photoaging parameters are as follows: the relative chamber humidity is 100%; the chamber and blackboard temperature were set to 36 and 40 °C, respectively; the lamp output power was fixed at 43% of the maximum power of 750 W; irradiance does is 0.34 W m^{-2}; the test time is 100 h.

Results and discussion

Characterizations of the prepared g-C_3N_4 nanosheets and the prepared g-C_3N_4 doped PBAT films

The crystallinity and morphology of the as-prepared g-C_3N_4 were characterized by XRD and TEM. As shown in Fig. 1a, two diffractions 2θ peaks at 12.9° and 27.7° are characteristic of (100) plans parallel to the *c*-axis and typical layer stacking of conjugated aromatic (002) planes, respectively.[31] The TEM images of the prepared g-C_3N_4 in Fig. 1b and S1† reveal the crinkly structure of the g-C_3N_4 nanosheets, with rough surfaces attributed to the gaseous template effect during high-temperature calcination. Subsequently, the light absorption properties of the prepared g-C_3N_4 were investigated by using UV-Vis DRS. As revealed in Fig. 1c, the prepared g-C_3N_4 exhibits light absorption in the wavelength range from 210 to 460 nm, covering the whole UV spectrum. Notably, the absorption coefficient of the g-C_3N_4 nanosheets exceeds 60% in the range of 310 to 400 nm, indicating their excellent UV light absorption capability. Accordingly, the band gap was estimated to be 2.85 eV by using the Tauc plot method, in agreement with the previous report.[32] Based on the above results, the prepared g-C_3N_4 nanosheets hold significant potential as an anti-aging additive for PBAT.

To see the applicability of the prepared g-C_3N_4 in PBAT, a calculated amount of g-C_3N_4 was weighted and incorporated into the PBAT film matrix by casting film method. For comparison, pure PBAT films and UV-0 doped PBAT films were also prepared using the same procedure. The average thickness of the resulting films is 28.64 μm for PBAT film, 26.82 μm for UV-0/PBAT, 26.53 μm for UV-0/PBAT, 26.80 μm for g-C_3N_4 (0.25)/PBAT, and 27.60 μm for g-C_3N_4 (0.5)/PBAT, respectively. Digital photos of the prepared films can be found in Fig. S2.† In comparison, the presence of UV-0 or g-C_3N_4 in PBAT film brings a deep yellow color and no obvious particles to the naked eye, indicating the successful incorporation of the UV absorber. To get a closer look at the prepared film, scanning transmission microscopy (SEM) was used to characterize the surface of the prepared g-C_3N_4-based PBAT films. As is shown, the surface of the pure PBAT film is smooth (Fig. 2a and b) while the g-C_3N_4 doped ones (Fig. 2c–f) are much more rough with visible cracks. These surface irregularities and cracks likely resulted from the aggregation of g-C_3N_4 nanosheets.

Then, FTIR spectra of the prepared films were collected in Fig. S3.† As displayed, all the prepared films exhibit similar typical PBAT peaks, and no obvious differences were observed due to the low loading amount and/or a better uniform distribution of the UV-0 and g-C_3N_4. For instance, the peak at 2951 cm^{-1} is assigned to the CH_3 and CH_2 stretch, the sharp peak at 1714 cm^{-1} originates from C=O stretching, and the peaks at 1101 cm^{-1}, 1267 cm^{-1}, and 726 cm^{-1} could be ascribed to the aromatic acid, $-CH_2-$, and C–O group, respectively.[33] The thermal degradation properties of the prepared films were also investigated under a nitrogen atmosphere (Fig. 3a and b). It can be seen that all the investigated films in this work exhibit similar onset degradation temperatures of 332.5 °C, the fastest degradation temperature is 415 °C. The presence of UV-0 or g-C_3N_4 in the PBAT matrix at this loading level has very little effect on the degradation properties of PBAT when considering the measurement error.

Photophysical properties of the prepared g-C_3N_4 doped PBAT films before aging and after aging

The UV-Vis absorption properties of the prepared films were analyzed by UV-Vis DRS. As shown in Fig. 4a, the reference pure PBAT shows its intrinsic strong UV absorption ability in the range of 200–314 nm, attributed to the absorption of the aromatic group in the PBAT backbone. While in the range of 320–400 nm, it exhibits almost no absorption. For the films UV-0 (0.25)/PBAT, UV-0 (0.5)/PBAT, g-C_3N_4 (0.25)/PBAT, and g-C_3N_4 (0.5)/PBAT, an additional broad absorption band in the range of 314–400 was observed which were come from the doped UV absorbers, indicating the successful introduction of UV-0 or g-C_3N_4 into the PBAT matrix. The absorption intensity of UV-0 or

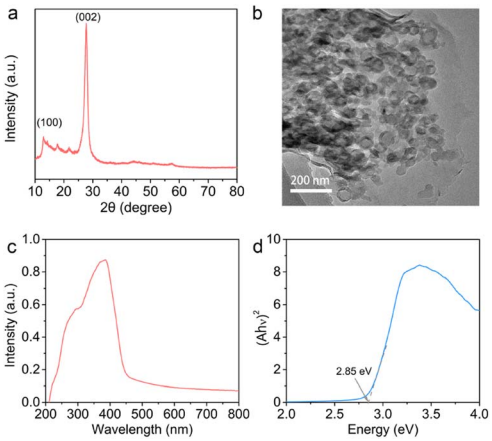

Fig. 1 (a) XRD patterns, (b) TEM image, (c) UV-Vis diffuse reflectance spectra, and (d) the corresponding Tauc plot of the prepared g-C_3N_4.

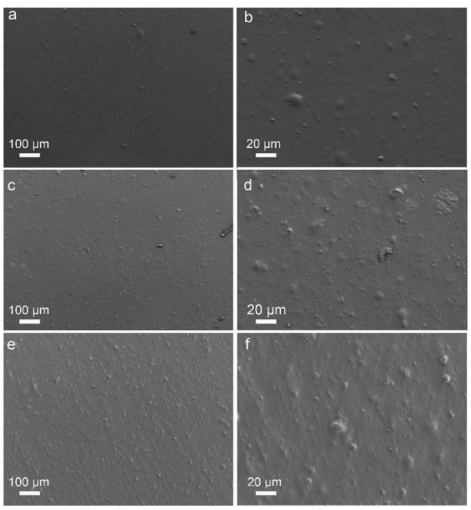

Fig. 2 SEM images of films (a and b) pure PBAT, (c and d) g-C_3N_4 (0.25)/PBAT, and (e and f) g-C_3N_4 (0.5)/PBAT.

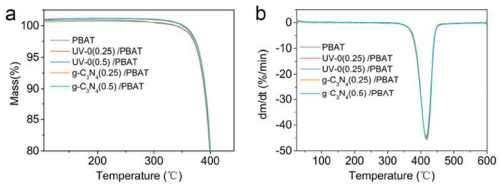

Fig. 3 (a) TGA curves and (b) DTG curves of films PBAT, UV-0 (0.25)/PBAT, UV-0 (0.5)/PBAT, g-C_3N_4 (0.25)/PBAT, and g-C_3N_4 (0.5)/PBAT, respectively.

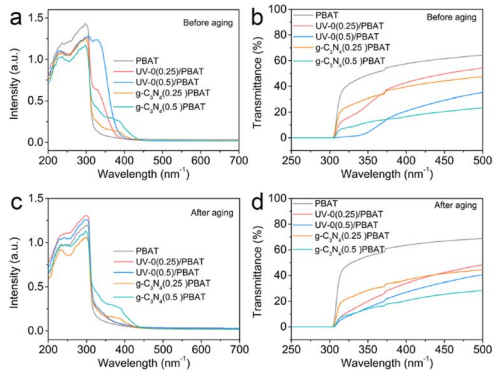

Fig. 4 (a) UV-Vis absorption spectra and (b) light transmittance rate spectra of the prepared films before photoaging. (c) UV-Vis absorption spectra and (d) light transmittance rate spectra of the prepared films after photoaging.

g-C_3N_4 contained PBAT films was increased linearly with the increase of UV absorber loading amount. In comparison, at the same doping amount level, PBAT films with UV-0 show a higher absorption intensity than those doped with g-C_3N_4 due to their difference in UV absorption density in the PBAT substrate. To be noted, the g-C_3N_4 doped PBAT films show an absorbance edge as far as 420 nm because of the visible light absorption capacity of g-C_3N_4. To further prove the good UV shielding ability of g-C_3N_4 doped PBAT films, the transmittance property of the prepared films was also studied. As shown in Fig. 4b, pure PBAT has the highest transmittance rate, with a transmittance level of 40–60% even in the UV range of 300–400 nm. However, the introduction of UV absorbers resulted in a significant light-blocking effect. For instance, the visible light transmittance rate decreases at least 10% of the film UV-0 (0.25)/PBAT over the whole visible light range, and less than 15% of UV light below 320 nm could penetrate the film. When the loading amount of UV-0 increases to 0.5 wt%, film UV-0 (0.5)/PBAT can shield almost all the UV light below 350 nm and more than 80% of the UV light in the range of 350–400 nm. The g-C_3N_4 doped PBAT films, also show a good ability to block the light in the UV region but less than the UV-0 one because of the lower number of UV absorption units, consistent with the UV-Vis absorption results. In the range of visible light, the g-C_3N_4 doped PBAT films showed a stronger light-blocking effect than the UV-0 films due to the particle reflecting the effect of the large g-C_3N_4 nanosheets. These results demonstrate that g-C_3N_4 can serve as a UV absorber similar to traditional UV-0 and has great potential to be a new type of UV absorber for biodegradable plastics.

To prove the g-C_3N_4 doped PBAT films have the potential for practical application in a real environment. The prepared films were aged in an aging chamber for 100 h. Subsequently, the UV-Vis absorption and light transmittance ability of the aged films were studied again. As shown in Fig. 4c, the absorption intensity in the range of 200–310 nm of pure PBAT film was largely decreased when compared with the freshly prepared one, indicating the molecular structure of PBAT was damaged due to UV light oxidation. In the case of UV-0-based PBAT film, we can see that the absorption band in the range of 310–400 nm almost disappeared, which means that UV-0 absorbers were unable to withstand such harsh conditions and became damaged, resulting in a loss of protection for PBAT. In stark contrast, g-C_3N_4-based PBAT films still show a similar UV shielding ability to that of the freshly prepared films, proving g-C_3N_4 possesses an ability of long service time as a UV absorber. The good UV shielding performance of g-C_3N_4 was further confirmed by comparing the light transmittance rate of the aged films. As revealed in Fig. 4d, the UV band light transmittance rate of the two aged UV-0-based PBAT films increased relative to the before-aging ones, while g-C_3N_4 contained ones exhibited no big difference before and after aging.

Mechanical properties of the prepared g-C_3N_4 doped PBAT films before aging and after aging

To see the effect of UV absorbers on the mechanical properties of the prepared PBAT films, we analyzed the tear strength, tensile strength, and elongation at the break of the freshly prepared (solid line) and those subjected to photooxidation aging (dash line). Initially, longitudinal studies were conducted on the films in this study. As is revealed in Fig. 5a–c, the mechanical properties are all UV absorber dependent, the introduction of UV-0 into the PBAT matrix brings a decrease of both tear and tensile strength and an enhancement of elongation at break, and this trend becomes much more distinct relative to pure PBAT when more UV-0 was loaded. Conversely, a reverse trend was observed for g-C_3N_4. In detail, the g-C_3N_4

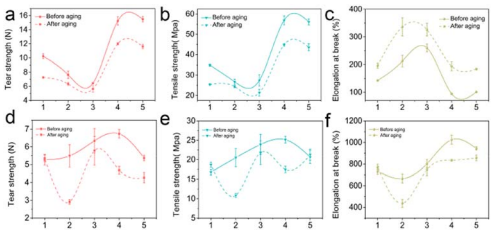

Fig. 5 (a) Longitudinal tear strength; (b) longitudinal tensile strength; (c) longitudinal elongation at break of the prepared films; (d) lateral tear strength; (e) lateral tensile strength; (f) lateral elongation at break of the prepared films. Numbers 1, 2, 3, 4, and 5 in the *x*-axis represent the investigated films PBAT, UV-0 (0.25)/PBAT, UV-0 (0.5)/PBAT, g-C_3N_4 (0.25)/PBAT, and g-C_3N_4 (0.5)/PBAT, respectively. Solid line: before photoaging. Dash line: after photoaging. Error bars show the standard deviation from three different tests.

(0.25)/PBAT and g-C_3N_4 (0.5)/PBAT have a tear strength of 15.24 and 15.48 N, respectively, which is almost 1.5 times that of pure PBAT. The tensile strength for pure PBAT is 34.9 MPa, then improved to the level of 56.0 MPa for both g-C_3N_4 (0.25)/PBAT and g-C_3N_4 (0.5)/PBAT. These results indicate that g-C_3N_4 shows the merits of a nanofiller for the reinforcement of polymeric materials, consistent with the reported works.[26] These enhancements could be explained by, the presence of g-C_3N_4, the traction force during the casting film process drives the crystallinity and non-crystallinity zone align along the tensile direction more efficiently. The decrease of the properties of elongation at break from 142 for pure PBAT to 94.7 for g-C_3N_4 (0.25)/PBAT (g-C_3N_4 (0.5)/PBAT is 100) could be attributed to the nanofiller effect of g-C_3N_4, resulting in more brittle PBAT films. After aging, as expected, all the aged films show a decline of tear strength and tensile strength to some extent, but much more for pure PBAT and g-C_3N_4-based PBAT films than for UV-0-based ones. Although a reduction of mechanical properties was observed in g-C_3N_4-based PBAT films, its value was still higher than the pure PBAT film without photoaging. In Fig. 5c, the plot shows the elongation at break properties for all the aged films, which are much larger than the original values. This phenomenon could be explained by the aging process deteriorating the polymer backbones of PBAT and reducing the crystallinity of the studied films, followed by an improved elongation at break. Furthermore, the lateral mechanical properties of the above-mentioned films were also investigated (Fig. 5d–f). In contrast to the longitudinal properties, the presence of UV-0 in the PBAT matrix leads to an increase in mechanical properties in all aspects when compared to pure PBAT. In the case of g-C_3N_4, the highest mechanical properties were achieved in the PBAT film with the loading amount of 0.25 wt%, followed by a declining trend with a loading amount set at 0.5 wt%. Likewise, all the aged films show a reduction of lateral mechanical properties after the aging process, but PBAT films with 0.5 wt% UV-0 are of the least due to their strong UV shielding ability.

Conclusions

In conclusion, g-C_3N_4 doped PBAT films have been successfully prepared by the casting film method. Pure PBAT and typical UV absorbers-based UV-0/PBAT films were prepared in the same way as the reference. UV-Vis absorption and light transmittance experiments show that g-C_3N_4/PBAT film can effectively absorb the incoming UV light relative to pure PBAT, g-C_3N_4 was found to play a similar role as a UV-0 absorber. The photo-aging results show that the UV shielding ability of the aged UV-0/PBAT films was largely decreased compared to fresh-prepared ones. In contrast, the aged g-C_3N_4/PBAT film still exhibited good UV absorption ability, highlighting the high stability of g-C_3N_4 compared to UV-0. Moreover, the merits of good mechanical properties of g-C_3N_4 are also manifested in the PBAT matrix, as the g-C_3N_4/PBAT composite films exhibited improved mechanical properties to some extent compared to pure PBAT and UV-0/PBAT films. This enhancement is particularly significant considering the poor mechanical properties of PBAT, which hinder its practical applications. It is worth noting that the improved UV shielding ability and mechanical properties of the g-C_3N_4/PBAT composite film studied in this work may not be as pronounced due to the relatively low loading amount and/or lack of elaborate modification of pristine g-C_3N_4. However, through this work, at least, the application of g-C_3N_4 to protect biodegradable plastic substrates was demonstrated. The advantages of g-C_3N_4 are successfully utilized. Undoubtedly, it is anticipated that more efficient g-C_3N_4-based UV shielding additives will be explored in the future through surface engineering or forming a hybrid composite with other materials.

Conflicts of interest

There are no conflicts to declare.

Acknowledgements

This work was supported by the Key Research and Development Task Project of Xinjiang Uygur Autonomous Region (2022B02033), the National Key Research and Development Program of China (No. 2021YFD1700700), the Agricultural Science and Technology Innovation Program of the Chinese Academy of Agricultural Sciences (2023), the Key Program for Science and Technology of CNTC (110202202030), and International Cooperation and Exchanges Project of National Natural Science Foundation of China and the Royal Society (No. 42311530066).

References

1 X. Zhao, B. Boruah, K. F. Chin, M. Đokić, J. M. Modak and H. S. Soo, Upcycling to Sustainably Reuse Plastics, *Adv. Mater.*, 2022, **34**, 2100843.
2 D. Sun, H. Li, E. Wang, W. He, W. Hao, C. Yan, Y. Li, X. Mei, Y. Zhang, Z. Sun, Z. Jia, H. Zhou, T. Fan, X. Zhang, Q. Liu, F. Wang, C. Zhang, J. Shen, Q. Wang and F. Zhang, An overview of the use of plastic-film mulching in China to increase crop yield and water-use efficiency, *Natl. Sci. Rev.*, 2020, **7**, 1523–1526.
3 Y. Liu, C. Zhao, C. Yan, L. Mao, Q. Liu, Z. Li and W. He, Effects of agricultural plastic film residues on transportation and distribution of water and nitrate in soil, *Chemosphere*, 2020, **242**, 125131.
4 S. Kubowicz and A. M. Booth, Biodegradability of Plastics: Challenges and Misconceptions, *Environ. Sci. Technol.*, 2017, **51**, 12058–12060.
5 J.-G. Rosenboom, R. Langer and G. Traverso, Bioplastics for a circular economy, *Nat. Rev. Mater.*, 2022, **7**, 117–137.
6 R. A. Chowdhury, M. Nuruddin, C. Clarkson, F. Montes, J. Howarter and J. P. Youngblood, The biodegradable polymer PBAT is hitting the big time, *Chemical & Engineering News*, 2021, vol. 99.
7 Q. Xing, P. Buono, D. Ruch, P. Dubois, L. Wu and W.-J. Wang, Biodegradable UV-Blocking Films through Core–Shell Lignin–Melanin Nanoparticles in Poly(butylene adipate-co-terephthalate), *ACS Sustain. Chem. Eng.*, 2019, **7**, 4147–4157.

8 C. Li, Z. Li and X. Ren, Preparation and characterization of polyester fabrics coated with TiO_2/benzotriazole for UV protection, *Colloids Surf., A*, 2019, **577**, 695–701.
9 D. J. Mendoza, C. Browne, V. S. Raghuwanshi, L. M. M. Mouterde, G. P. Simon, F. Allais and G. Garnier, Phenolic Ester-Decorated Cellulose Nanocrystals as UV-Absorbing Nanoreinforcements in Polyvinyl Alcohol Films, *ACS Sustain. Chem. Eng.*, 2021, **9**, 6427–6437.
10 Y. Wang, J. Su, T. Li, P. Ma, H. Bai, Y. Xie, M. Chen and W. Dong, A Novel UV-Shielding and Transparent Polymer Film: When Bioinspired Dopamine–Melanin Hollow Nanoparticles Join Polymers, *ACS Appl. Mater. Interfaces*, 2017, **9**, 36281–36289.
11 S. Heo, H. S. Hwang, Y. Jeong and K. Na, Skin protection efficacy from UV irradiation and skin penetration property of polysaccharide-benzophenone conjugates as a sunscreen agent, *Carbohydr. Polym.*, 2018, **195**, 534–541.
12 Z. Huang, A. Ding, H. Guo, G. Lu and X. Huang, Construction of Nontoxic Polymeric UV-Absorber with Great Resistance to UV-Photoaging, *Sci. Rep.*, 2016, **6**, 25508.
13 M. Rani, W. J. Shim, G. M. Han, M. Jang, Y. K. Song and S. H. Hong, Benzotriazole-type ultraviolet stabilizers and antioxidants in plastic marine debris and their new products, *Sci. Total Environ.*, 2017, **579**, 745–754.
14 S. Kim, T. G. Hwang, J. W. Namgoong, H. M. Kim and J. P. Kim, Effect of linker moiety on linear dimeric benzotriazole derivatives as highly stable UV absorber for transparent polyimide film, *Dyes Pigm.*, 2020, **180**, 108469.
15 X. Sun, K. Wang, H. Liu, Y. Zhao, Y. Li and D. Xie, One-Pot Preparation of Benzotriazole-Modified Porous Silica for Durable UVA Absorption Ability, *ACS Omega*, 2022, **7**, 1113–1120.
16 A. Sahar, S. Ali, T. Hussain, M. Irfan, B. Eliasson and J. Iqbal, UV absorbers for cellulosic apparels: A computational and experimental study, *Spectrochim. Acta, Part A*, 2018, **188**, 355–361.
17 M. Zayat, P. Garcia-Parejo and D. Levy, Preventing UV-light damage of light sensitive materials using a highly protective UV-absorbing coating, *Chem. Soc. Rev.*, 2007, **36**, 1270–1281.
18 S. V. Nguyen and B.-K. Lee, PVA/CNC/TiO_2 nanocomposite for food-packaging: improved mechanical, UV/water vapor barrier, and antimicrobial properties, *Carbohydr. Polym.*, 2022, **298**, 120064.
19 E. Olson, Y. Li, F.-Y. Lin, A. Miller, F. Liu, A. Tsyrenova, D. Palm, G. W. Curtzwiler, K. L. Vorst, E. Cochran and S. Jiang, Thin Biobased Transparent UV-Blocking Coating Enabled by Nanoparticle Self-Assembly, *ACS Appl. Mater. Interfaces*, 2019, **11**, 24552–24559.
20 W. Wang, B. Zhang, S. Jiang, H. Bai and S. Zhang, Use of CeO_2 Nanoparticles to Enhance UV-Shielding of Transparent Regenerated Cellulose Films, *Polymers*, 2019, **11**, 458.
21 B. Sreenivasulu, B. R. Ramji and M. Nagaral, A Review on Graphene Reinforced Polymer Matrix Composites, *Mater. Today: Proc.*, 2018, **5**, 2419–2428.
22 Y. Cui, S. I. Kundalwal and S. Kumar, Gas barrier performance of graphene/polymer nanocomposites, *Carbon*, 2016, **98**, 313–333.
23 S. Karimi, E. Helal, G. Gutierrez, N. Moghimian, M. Madinehei, E. David, M. Samara and N. Demarquette, A Review on Graphene's Light Stabilizing Effects for Reduced Photodegradation of Polymers, *Crystals*, 2021, **11**, 1–22.
24 Y. Moon, J. Yun, H. I. Kim and Y. S. Lee, Effect of graphite oxide on photodegradation behavior of poly(vinyl alcohol)/graphite oxide composite hydrogels, *Carbon Lett.*, 2011, **12**, 138–142.
25 G. Navaneethakrishnan, N. Parthipan and K. Chellamuthu, Effects of g-C_3N_4 on mechanical and thermal properties of epoxy nanocomposites, *Mater. Today: Proc.*, 2022, **69**, 962–966.
26 Y. Shi, S. Jiang, K. Zhou, C. Bao, B. Yu, X. Qian, B. Wang, N. Hong, P. Wen, Z. Gui, Y. Hu and R. K. K. Yuen, Influence of g-C_3N_4 Nanosheets on Thermal Stability and Mechanical Properties of Biopolymer Electrolyte Nanocomposite Films: A Novel Investigation, *ACS Appl. Mater. Interfaces*, 2014, **6**, 429–437.
27 Y. N. Baghdadi, J. Sinno, K. Bouhadir, M. Harb, S. Mustapha, D. Patra and A. R. Tehrani-Bagha, The mechanical and thermal properties of graphitic carbon nitride (g-C_3N_4)-based epoxy composites, *J. Appl. Polym. Sci.*, 2021, **138**, 51324.
28 B. Mortazavi, G. Cuniberti and T. Rabczuk, Mechanical properties and thermal conductivity of graphitic carbon nitride: A molecular dynamics study, *Comput. Mater. Sci.*, 2015, **99**, 285–289.
29 W.-J. Ong, L.-L. Tan, Y. H. Ng, S.-T. Yong and S.-P. Chai, Graphitic Carbon Nitride (g-C_3N_4)-Based Photocatalysts for Artificial Photosynthesis and Environmental Remediation: Are We a Step Closer To Achieving Sustainability?, *Chem. Rev.*, 2016, **116**, 7159–7329.
30 X. Lu, K. Xu, P. Chen, K. Jia, S. Liu and C. Wu, Facile one step method realizing scalable production of g-C_3N_4 nanosheets and study of their photocatalytic H_2 evolution activity, *J. Mater. Chem. A*, 2014, **2**, 18924–18928.
31 W. Iqbal, B. Qiu, J. Lei, L. Wang, J. Zhang and M. Anpo, One-step large-scale highly active g-C_3N_4 nanosheets for efficient sunlight-driven photocatalytic hydrogen production, *Dalton Trans.*, 2017, **46**, 10678–10684.
32 J. Zhang, M. Zhang, G. Zhang and X. Wang, Synthesis of Carbon Nitride Semiconductors in Sulfur Flux for Water Photoredox Catalysis, *ACS Catal.*, 2012, **2**, 940–948.
33 L. Lai, S. Wang, J. Li, P. Liu, L. Wu, H. Wu, J. Xu, S. J. Severtson and W.-J. Wang, Stiffening, strengthening, and toughening of biodegradable poly(butylene adipate-co-terephthalate) with a low nanoinclusion usage, *Carbohydr. Polym.*, 2020, **247**, 116687.